



Published in final edited form as:

Inhal Toxicol. 2011 July ; 23(8): 495–505. doi:10.3109/08958378.2011.587034.

Laboratory evaluation of a prototype photochemical chamber designed to investigate the health effects of fresh and aged vehicular exhaust emissions

Vasileios Papapostolou, Joy E. Lawrence, Edgar A. Diaz, Jack M. Wolfson, Stephen T. Ferguson, Mark S. Long, John J. Godleski, and Petros Koutrakis

Department of Environmental Health, Harvard School of Public Health, Boston, Massachusetts, USA

Abstract

Laboratory experiments simulating atmospheric aging of motor vehicle exhaust emissions were conducted using a single vehicle and a photochemical chamber. A compact automobile was used as a source of emissions. The vehicle exhaust was diluted with ambient air to achieve carbon monoxide (CO) concentrations similar to those observed in an urban highway tunnel. With the car engine idling, it is expected that the CO concentration is a reasonable surrogate for volatile organic compounds (VOCs) emissions. Varying the amount of dilution of the exhaust gas to produce different CO concentrations, allowed adjustment of the concentrations of VOCs in the chamber to optimize production of secondary organic aerosol (SOA) needed for animal toxicological exposures. Photochemical reactions in the chamber resulted in nitric oxide (NO) depletion, nitrogen dioxide (NO₂) formation, ozone (O₃) accumulation, and SOA formation. A stable SOA concentration of approximately 40 μg m⁻³ at a chamber mean residence time of 30 min was achieved. This relatively short mean residence time provided adequate chamber flow output for both particle characterization and animal exposures. The chamber was operated as a continuous flow reactor for animal toxicological tests. SOA mass generated from the car exhaust diluted with ambient air was almost entirely in the ultrafine mode. Chamber performance was improved by using different types of seed aerosol to provide a surface for condensation of semivolatile reaction products, thus increasing the yield of SOA. Toxicological studies using Sprague-Dawley rats found significant increases of *in vivo* chemiluminescence in lungs following exposure to SOA.

Keywords

Photochemical chamber; secondary organic aerosol; vehicular emissions

Introduction

Epidemiological studies have shown associations between exposures to ambient particles and adverse health outcomes, such as cardiopulmonary morbidity and mortality (Dockery et al., 1993; Dockery & Pope, 1994; Pope et al., 2002; Schwartz, 2004). Because ambient particles originate from many different sources, with associated differences in composition

© 2011 Informa Healthcare USA, Inc.

Address for Correspondence: Department of Environmental Health, Harvard School of Public Health, 401 Park Drive, Boston, Massachusetts 02215, USA. vpapapos@hsph.harvard.edu.

Declaration of interest The authors report no declarations of interest.

and physicochemical characteristics, it is likely that there are corresponding differences in toxicity. Mobile source emissions are a significant contributor to individual and community exposures, and are of substantial interest in health effect studies. Laden et al. (2000) showed that direct vehicular emissions were associated with increased rate of cardiovascular deaths. Another study showed an association between transient exposure to traffic emissions and an increase in the risk of myocardial infarction (Peters et al., 2004).

Although epidemiological studies can examine associations between population exposures and outcomes, there is still a need to study the effects of exposure to particulate pollutants from specific sources. So far, most research has focused on measurements of the toxicity of particles directly emitted from combustion sources. For example, exposure to directly emitted diesel particles has been associated with lung infection or inflammation and oxidative stress in mice (McDonald et al., 2004). In a toxicological study, exposure to gasoline vehicle emissions was associated with cell damage (Seagrave et al., 2003).

Ambient aerosol consists of a complex mixture of both directly emitted particles (primary) and those formed in the atmosphere through photochemical reactions (secondary) (Lim & Turpin, 2002). This raises questions about how the toxicity of pollution emitted from different sources is affected by atmospheric transformations. Recently, there have been a few studies that have begun to look at this question. The TERESA (Toxicological Evaluation of Realistic Emission Source Aerosols) study (Godleski et al., 2011; Godleski et al., 2011; Kang et al., 2011) investigated the toxicity of primary and simulated secondary emissions from coal-fired power plants. Other researchers investigated the toxicological properties of secondary aerosol from a diesel generator (Zielinska et al., 2010).

Vehicular primary emissions include elemental carbon (EC) particles (primarily from diesel vehicles) as well as road and brake dust and other fugitive emissions. However, vehicular pollutants also include pollutant gases such as carbon monoxide (CO), oxides of nitrogen (NO_x), mostly in the form of nitric oxide (NO), volatile organic compounds (VOCs), and semivolatile organic compounds (SVOCs) as evaporative losses from the fuel and from engine lubricants.

In the presence of sunlight, primary pollutant gases react with ozone (O_3), hydroxyl radical ($\cdot\text{OH}$), or other radicals. Inorganic gases are converted into secondary pollutant particles such as ammonium nitrate (NH_4NO_3) and ammonium sulfate ($[\text{NH}_4]_2\text{SO}_4$), while VOCs are converted into secondary organic aerosol (SOA) through photochemical reactions. SOA is formed mostly by oxidation of VOC species with 7 or more carbons to produce reaction products that subsequently partition between gas and particle phase (Seinfeld & Pandis, 2006).

Although substantial amounts of both gas- and particle-phase gases in primary emissions are oxidized, they produce relatively low yields of SOA. Particulate phase organics such as polycyclic aromatic hydrocarbons (PAHs) are products of both incomplete combustion and pyrolysis of fuel and/or lubricant. In the atmosphere, these PAHs are oxidized to form predominantly particle-phase nitro- and oxy-PAH derivatives (Nikolaou et al., 1984; Finlayson-Pitts, 1986; Seinfeld & Pandis, 2006). Even those PAH reactions that do not result in particle-phase products can have a significant impact on the toxic or genotoxic potency of particles (Feilberg et al., 2002).

A large number of laboratory chamber studies (Izumi & Fukuyama, 1990; Odum et al., 1997a, 1997b; Cocker et al., 2001a; Kleindienst et al., 1999; Kleindienst et al., 2004; Ng et al., 2006) have investigated the SOA-forming potential of individual aromatic hydrocarbons and mixtures typical of mobile source emissions, which comprise the major component of

the precursors of SOA in urban areas. Kleindienst et al. (1999) found that toluene achieved the highest SOA yield, followed by *p*-xylene and 1–3–5 trimethylbenzene.

This paper presents the laboratory development and optimization of a prototype dynamic photochemical chamber that produces sufficient amounts of SOA from VOCs in car exhaust of a single vehicle under irradiation with artificial light. It was the purpose of this study to demonstrate the ability to detect biological outcomes of exposure to SOA produced by a single vehicle, in animal toxicological studies. The aim was not to fully simulate the whole spectrum of atmospheric photochemical reaction products that are formed in the real ambient atmosphere. The same degree of oxidation that occurs in the atmosphere cannot be truly recreated in a photochemical reaction chamber using artificial light because, as it is known, photochemical chambers generally produce a less oxidized aerosol and smaller yield than can be found in the atmosphere. However, for toxicological testing, the reproducibility offered by artificial lighting compared to actual solar irradiation (which can vary in intensity by hour and by day) is desirable because it affords reproducible products from reproducible gas-phase mixtures. This is especially true for inhalation toxicology studies, where stable production and output are required over an exposure period of several hours, using a dynamic system. Results from the prototype tests were used to design a planned follow-up study of the toxicity of similarly aged realistic aerosol derived from mobile source emissions from an urban traffic tunnel.

Methods

Photochemical chamber

The photochemical reaction chamber (Ruiz et al., 2007a) previously used for a TERESA coal-fired power plant study (Ruiz et al., 2007b; Kang et al., 2010) was used to simulate the atmospheric photochemical aging of motor vehicle exhaust diluted with ambient air.

The design and manufacture of the chamber are described in detail elsewhere (Ruiz et al., 2007a). This rectangular shaped 0.575 m³ chamber has an FEP (fluorinated ethylene propylene) Teflon-coated aluminum framework. The chamber has a floor area of 1.52 × 0.31 m² and a 1.22 m height achieving a relatively low surface (*S*) to volume (*V*) ratio of $S \times V = 9.4 \text{ m}^{-1}$ to minimize particle losses. FEP Teflon film with thickness of 51 μm (American Durafilm, Holliston, MA) was used on the two larger sides of the framework to allow irradiation to penetrate into the chamber. PTFE (polytetrafluoro-ethylene) Teflon was used on the four smaller sides to minimize wall reactions. A ventilated wooden enclosure was used to protect researchers from exposure to ultraviolet (UV) light and to remove excess heat generated by the lamps. A total of 48 UVA-340 20 W lamps (Q-Panel Lab Products, Cleveland, OH) were mounted on two enclosure sides at a distance of about 5×10^{-2} from the chamber walls.

The UVA-340 lamps, with a strong photon emission around 340 nm, provide an excellent simulation of the ground level solar spectrum (between 295 nm and 365 nm) (Carter, 1995). The stable UV radiation of these lamps enhances the photolysis of O₃, nitrous acid (HONO), and formaldehyde (HCHO), with moderate heat release.

Emission generation and sampling

The laboratory experimental system is shown schematically in Figure 1. A compact automobile (1997 Toyota RAV4, SUV) was used as a source of emissions. The engine was run slightly fuel-rich by controlling the vacuum at the Manifold Absolute Pressure sensor during experiments, causing a slight decrease in the efficiency of fuel combustion and resulting in CO concentrations (after dilution with ambient air) similar to those observed in a highway tunnel (Rogak et al., 1998; Kirchstetter et al., 1996; Fraser et al., 1999; Fraser et

al., 1998; Pierson et al., 1996). We considered it reasonable to adjust the levels of inefficiency of fuel combustion to achieve CO levels comparable to CO levels observed in mobile source fleet emissions at an urban highway tunnel e.g. 2–12 ppm. Also, the CO would be a qualitative indicator of the amount of VOCs concentration in the mixture introduced in the chamber, e.g. low CO–low VOCs, high CO–high VOCs. Thus, we expected that the CO served as a reasonable surrogate for VOCs emissions (Fraser et al., 1998).

The car was parked in between buildings of the Harvard School of Public Health and the Harvard School of Dental Medicine in the Longwood Medical Area in Boston, MA. The tailpipe was inserted into a tube that captured all of the exhaust from the tailpipe plus outdoor air (primary dilution of the exhaust with cooling to near ambient temperature). The mixture was pulled by a variable speed fan through a duct (length about 30 ft) into the laboratory. Most of the mixture was vented to a fume hood in the laboratory, with a small amount transferred by a vacuum pump to the reaction chamber. Before entering the chamber, a secondary dilution of the exhaust mixture was made with outside ambient air.

Measurement and monitoring

Continuous gas monitors were used to monitor the concentrations entering and exiting the chamber, with a 4-way to automatically switch at 5-min intervals between upstream and downstream. CO was monitored by infrared absorption (Model 48 Analyzer; Thermo Scientific, Franklin, MA), NO and NO₂ by chemiluminescence (Model 42C Analyzer; Thermo Scientific), O₃ by UV photometry (Model 49C Analyzer; Thermo Scientific).

Particle size distribution and concentration were monitored using a Scanning Mobility Particle Sizer (SMPS Model 3934; TSI Inc., Shoreview, MN) coupled with a Condensation Particle Counter (CPC Model 3785; TSI Inc.) and an Aerodynamic Particle Sizer (APS Model 3321; TSI Inc.). Particle count was monitored using a Condensation Particle Counter (CPC Model 3007; TSI Inc.). Particle mass concentration was estimated using the SMPS, assuming spherical particles and estimated particle density ($\rho_p = 1.0 \text{ g cm}^{-3}$) for SOA. Particle instruments were connected directly to the outlet of the chamber with short pieces of tubing to minimize particle losses.

Temperature and relative humidity were monitored using a Vaisala transmitter (HMD-70; Vaisala Oyj, Helsinki, Finland). The sensor was placed inside the enclosure, just outside of the chamber. A flow of 0.3 L min^{-1} was taken from the chamber and passed over the sensor probe.

VOC samples were collected in a subset of experiments on duplicate stainless steel TD (thermal desorption), unconditioned Carbopack B tubes (Supelco Division; Sigma-Aldrich Co) that were subsequently analyzed by gas chromatography/mass spectrometry (GC/MS). The tubes were sampled upstream and downstream of the chamber, at a flow rate of $20 \text{ cm}^3 \text{ min}^{-1}$ for 120 min. The flow rate through each tube was adjusted by a valve and flow stability was continuously monitored during each experiment using a vacuum gauge to measure the pressure drop.

Typical experimental protocol

Unless otherwise indicated, the experimental protocol was: (1) flush overnight with ambient air; (2) in the morning of the day of the experiment, start car and adjust CO concentration in exhaust by adjusting primary and secondary dilutions; (3) connect diluted exhaust to chamber and establish the desired mean residence time by adjusting the flow through the chamber; (4) wait for steady CO concentration in the chamber at target level (typically 2 mean residence times); (5) turn on lamps, and; (6) leave lamps on for duration of the

experiment (typically 5 mean residence times). In the seed aerosol experiments, addition and subsequent stabilization of the seed aerosol concentration preceded the irradiation of the chamber.

EC/OC tests

Three sets of experiments were conducted (see Table 2) by varying the diluted car exhaust CO concentration and the mean residence time in the chamber. When a stable CO concentration, exiting the chamber, was reached, either 10 or 20 ppm, the lamps were turned on and the photochemical reactions that involved oxidation of vehicular precursor gas-phase compounds took place. In combination with the different CO concentrations, two different flow rates were also tested, either 20 or 10 L min⁻¹, resulting in 30 or 60 min mean residence time in the chamber, respectively. Samples for EC/organic carbon (OC) analysis were collected upstream and downstream of the chamber. The sample flow through the filters was started when the lamps were turned on and was stopped at the end of the experiment. The chamber irradiation experiments lasted for 4 h. The filters used for EC/OC collection were 47 mm pre-fired quartz (Sunset Lab. Inc., Tigard, OR) placed in PFA Teflon filter holders (Savillex, Minnetonka, MN). It should be noted that all samples for EC/OC analysis were collected during experiments where only diluted car exhaust was photochemically oxidized in the chamber with no artificial aerosol added. The filters were subsequently stored in a freezer and later analyzed in our laboratory facilities using the IMPROVE-TOR (Thermal Optical Reflectance) method (Chow et al., 1993) using our Sunset OCEC Dual-Optical Lab Analyzer (Sunset Lab. Inc.).

Seed aerosol tests

Formation of SOA was also studied in the presence of different types of inert seed aerosol. The seed aerosol was added for three reasons: (1) to provide sufficient particle surface area to allow rapid aggregation of the freshly generated ultrafine SOA particles and condensation of gases, resulting in improved secondary PM yield; (2) to decrease the time required to form a stable accumulation mode size distribution; and (3) to achieve PM concentrations similar to those found in an urban highway tunnel in the northeastern United States.

The seed aerosol was generated (from an aqueous dispersion) with a HEART (High-output Extended Aerosol Respiratory Therapy; Westmed, Inc, Tucson, AZ) nebulizer. The output of the nebulizer was diluted with particle-free dry air in a 4-L vessel. The aerosol was then mixed with the diluted car exhaust in the chamber. Following stabilization of the CO concentration in the chamber, addition of the seed aerosol was started. When a steady-state baseline seed aerosol mass concentration was reached the lamps were turned on to initiate the photochemical reactions.

One set of experiments used hollow glass spheres (HGS; diameter, $d = 2\text{--}20\ \mu\text{m}$; density, $\rho_p = 1.1\ \text{g cm}^{-3}$; Polysciences Inc., Warrington, PA), which is chemically rather inert. Another set of experiments used Mt Saint Helens Ash (MSHA; density, $\rho_p = 2.6\ \text{g cm}^{-3}$), which is both chemically and toxicologically inert (Savage et al., 2003).

Well-mixed chamber- Particle losses tests

The chamber was filled at a flow of 5 L min⁻¹ with car exhaust diluted with ambient air at 20 ppm of CO. Particle and gas concentrations exiting the chamber were stabilized after a 2-h period and the lamps were turned on. After 4 h of elapsed irradiation time (2 mean residence times) the lamps were turned off. By that time there was a stable chamber concentration of secondary aerosol. At that point, the flow into the chamber was lowered from 5 L min⁻¹ to roughly 2.2 L min⁻¹, substituting clean, particle-free air for diluted car exhaust. This flow of 2.2 L min⁻¹ was sufficient to replace the total flow sampled

downstream of the chamber through the gas/particle instruments. The CO monitor, at 1.1 L min⁻¹, was used to measure the CO concentration. The SMPS, at 0.3 L min⁻¹, was used to measure the particle mass concentration assuming spherical particles and particle density of $\rho_p = 1.0 \text{ g cm}^{-3}$. The CPC, at 0.77 L min⁻¹, was used to measure particle number concentrations. The clean air flow (2.2 L min⁻¹) going into the chamber (slightly higher than the sum of the instrumental flows, 2.17 L min⁻¹) was used to slightly pressurize the chamber and prevent convex distortion of the Teflon film walls (with the very small excess flow released through small leaks in the chamber). This flow through the chamber approximated static mode conditions (negligible flow relative to chamber volume). Measurements were taken at 5-min intervals with the three instruments. This experimental setup was used to test whether the reaction chamber behaved as a wellmixed chamber and also to estimate the particle losses in the chamber.

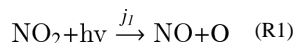
Determination of NO₂ photolysis rate

We determined the NO₂ photolysis rate in the chamber by steady-state actinometry (Cocker et al., 2001b). A mixture of NO and O₃ in clean, particle-free air was introduced continuously into the chamber. When a stable NO₂ concentration was reached, the lamps were turned on and the NO₂ photolysis rate (j_1) was calculated using the photostationary state relationship of NO, NO₂, and O₃ (Equation (1)):

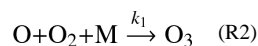
$$j_1 = k_2 \frac{[\text{NO}] \cdot [\text{O}_3]}{[\text{NO}_2]} \quad (1)$$

where $k_2 = 3.0 \times 10^{-12} \times \exp(-1500 \times T^{-1}) \text{ cm}^3 \text{ molecule}^{-1} \text{ s}^{-1}$ (with gas concentrations in molecules⁻¹ s⁻¹), the temperature (T in degrees K) dependent rate constant for the reaction of NO with O₃ (Sander et al., 2003).

Equation (1) was derived from reactions R1-R3:



Reaction R1 describes the photolysis of NO₂ at wavelengths $\lambda < 424 \text{ nm}$



Reaction R2 describes the reaction (with rate constant k_1) of the oxygen atom with the oxygen molecule to form ozone (M is O₂ or N₂ that absorbs excess energy to stabilize O₃), and:



Reaction R3 describes the reaction (with rate constant k_2) of O₃ with NO to regenerate NO₂.

At the photostationary state,

$$\frac{d[\text{O}_3]}{dt} = 0 = k_1 \cdot [\text{O}] \cdot [\text{O}_2] \cdot [\text{M}] - k_2 \cdot [\text{NO}] \cdot [\text{O}_3] \quad (2)$$

and

$$\frac{d[\text{O}]}{dt} = 0 = j_1 \cdot [\text{NO}_2] - k_1 \cdot [\text{O}] \cdot [\text{O}_2] \cdot [\text{M}] \quad (3)$$

Thus,

$$[\text{O}_3]_{\text{ss}} = \frac{\{k_1 \cdot [\text{O}] \cdot [\text{O}_2] \cdot [\text{M}]\}}{\{k_2 \cdot [\text{NO}]\}} \quad (4)$$

and

$$[\text{O}]_{\text{ss}} = \frac{\{j_1 \cdot [\text{NO}_2]\}}{\{k_1 \cdot [\text{O}_2] \cdot [\text{M}]\}} \quad (5)$$

Substituting,

$$[\text{O}_3]_{\text{ss}} = \frac{\{j_1 \cdot [\text{NO}_2]\}}{\{k_2 \cdot [\text{NO}]\}} \quad (6)$$

and rearranging, equation 1 is developed.

Toxicological studies

Animals—Male Sprague-Dawley (SD-CD) rats 250–350g were obtained from Taconic Farms (Rensselaer, NY); housed and managed according to NIH guidelines for the care and use of laboratory animals. Upon arrival, animals were randomly assigned a unique identification number which determined the exposure group.

Experimental design—Two different exposure scenarios were evaluated: (1) MSHA; (2) MSHA+SOA and these were compared to filtered air (Sham) exposures. For any given day of exposures, 2 SD-CD rats were exposed to aerosol and 2 to filtered room air in the individual whole-body exposure chambers for 6 h. At the end of the exposure, animals from each group had chemiluminescence studies of the heart and lung (Gurgueira et al., 2002).

Exposure—Tailpipe emissions from the car were collected and diluted with ambient air as described above. The chamber was operated dynamically, with residence time in the chamber optimized for the production of secondary PM from the exhaust. We also verified that the production of secondary particle mass was consistent for the specific concentration of CO in the diluted exhaust. MSHA was used as a seed aerosol (see Section *Seed aerosol effect*). Excess primary and photochemical gases from the photochemical chamber were removed before exposure using a countercurrent membrane diffusion denuder (Ruiz et al., 2006).

Organ chemiluminescence—Spontaneous chemiluminescence of the surface of lung and heart was measured as previously described (Gurgueira et al., 2002). Briefly, a Thorn EMI CT1 single-photon counting apparatus with an EMI 9816B photomultiplier cooled at -20°C was used. Rats were anesthetized with sodium pentobarbital (50 mg kg^{-1} i.p.) and connected to an animal ventilator (5 ml breath^{-1} , $60 \text{ breaths min}^{-1}$; Harvard Apparatus, Cambridge, MA), the chest was opened and the animals were placed in the measurement compartment. Body temperature was kept at 37°C using isothermal pads (Braintree Scientific, Braintree, MA). Emission data were expressed as counts per second per unit of tissue surface (cps cm^{-2}). Statistical analyses used analysis of variance models to assess an exposure effect on the mean and to compare the exposure effects across different scenarios.

Results and discussion

Determination of NO₂ photolysis rate

The magnitude of light irradiation by the UVA-340 lamps surrounding the chamber was estimated by measuring the NO₂ photolysis rate (j_1), which we determined experimentally to be $j_1 = 0.18 \text{ min}^{-1}$ (using Equation (1)). Using banks of UVB-313 lamps (in contrast with the UVA-340 lamps for these experiments) with this same chamber, Ruiz et al. (2006) measured $j_1 = 0.096 \text{ min}^{-1}$. As indicated by Carter et al. (1995), the ideal light irradiation for a photochemical chamber would correspond to approximately $j_1 = 0.3 \text{ min}^{-1}$, which is approximately 50% of the maximum NO₂ photolysis rate observed at ground level (at mid-US latitudes) on a clear day with direct overhead sunlight. For example, Zafonte et al. (1977) estimated $j_1 = 0.45 \text{ min}^{-1}$ in Los Angeles at noon time.

Well-mixed chamber—particle losses test

We introduced a small flow of clean particle-free air into the chamber, containing a stable concentration of CO and particles and measured the concentration of CO and particles downstream of the chamber for several hours.

Equation (8) was used to calculate the theoretical decay curve due to dilution only in the chamber.

$$\frac{C_{(t)}}{C_{(0)}} = \exp \cdot (-kt) \quad (7)$$

where the ratio $C_{(t)}/C_{(0)}$ is the remaining fraction as a dimensionless parameter in the chamber; k is the loss rate constant or the reciprocal of the mean residence time in the chamber, where $k = F \times V^{-1}$, in min^{-1} (F : flow rate; V : volume).

Using the nominal chamber volume ($V = 0.575 \text{ m}^3$) and the dilution clean air flow rate ($F = 2.2 \text{ L min}^{-1}$) the theoretical decay curve k value was calculated to be $k = 3.8 \times 10^{-3} \text{ min}^{-1}$. Figure 2 also shows the experimental CO decay curve over time in the chamber. Because CO is relatively inert, losses in the chamber may be due to dilution only. The experimental CO decay curve was exponential, the k value was calculated to be $k = 4.0 \times 10^{-3} \text{ min}^{-1}$. The excellent agreement between the experimental CO decay curve and the theoretical curve due to dilution only confirmed that this chamber behaved as a well-mixed flow reactor.

The decay of the particle mass and particle count as measured by the SMPS and the CPC, respectively, are also shown in Figure 2. The experimental particle mass decay curve was exponential, with a value of $k = 5.1 \times 10^{-3} \text{ min}^{-1}$. This larger value of k indicates that there are particle mass losses onto the chamber wall surfaces, in addition to dilution. The maximum observed losses of particle mass in the chamber were around 22%. The experimental particle count decay curve was also exponential, with a value of $k = 7.0 \times 10^{-3} \text{ min}^{-1}$. This even larger value of k indicates that in addition to dilution and losses onto the chamber wall surfaces, particle count losses may also be due coagulation of freshly formed ultrafine particles to form larger particles.

The particle count CPC predominantly measures ultrafine particles (below 100 nm), which can be lost by Brownian diffusion to chamber walls and by coagulation with other particles, and by electrostatic effects. The particle mass SMPS measurements are dominated by somewhat larger particles (since mass is proportional to the cube of the diameter). Like the ultrafine particles, these larger particles, having a diameter between 100 nm and 1 μm , can be lost by electrostatic effects (McMurry & Rader, 1985), but with lower losses by diffusion and coagulation, and, in addition, they can be lost due to gravitational settling (Crump &

Seinfeld, 1981; Pierce et al., 2008). These mechanisms can explain why the count and mass decay curves show more losses than by dilution alone. Ruiz et al. (2007a) used results from his pilot chamber particle losses tests using an artificial monodisperse aerosol to mathematically estimate the particle losses in the chamber using a simple box model and assuming a well-mixed flow reactor. Using this approach, Ruiz et al. (2007a) estimated losses of 32, 47, and 23% for particles around 50, 100, and 500 nm in size, respectively.

Gas-phase reactions

Tests with car exhaust diluted to 10 and 20 ppm of CO were conducted at 20 L min^{-1} (corresponding to a chamber mean residence time of approximately 30 min). Once a steady-state CO concentration was reached in the chamber, the lamps were turned on to initiate photochemical reactions, quickly followed by formation of SOA in the chamber.

Photochemical oxidation of the diluted car exhaust followed a fairly typical pattern, with rapid conversion of NO to NO₂, followed by accumulation of O₃. Typical results from an experiment with 20 ppm of CO introduced in the chamber are presented in Figure 3.

Only a few minutes after the lamps were turned on, the initial amount of NO was completely titrated and NO₂ (measured by the chemiluminescence analyzer as NO_x-NO) started forming rapidly. O₃ accumulated rapidly in the chamber reaching an average of 350 ppb after 240 min. The NO_x-NO concentration that included a high fraction in the form of NO₂ was on average 150 ppb over the course of the experiment.

Note that free radical formation in our chamber was initiated without addition of any accelerant. In the Ruiz et al. (2007a) study, as there were virtually no VOCs in the diluted power plant stack gas, it was necessary to add O₃ to first titrate the relatively high amount of NO. Also, O₃ was added to produce high concentrations of ·OH (by photolysis of O₃ using UVB-313 lamps) in order to oxidize sulfur dioxide (SO₂) in coal-fired power plant emissions. The reactions in our chamber resulted in a relatively high O₃ accumulation without any accelerant because the amounts of aromatic hydrocarbons, among the total VOCs, were relatively high. These compounds, as well as their major photochemical oxidation products, undergo photolysis to generate free radicals (Seinfeld & Pandis, 2006).

SOA formation

Under the same conditions discussed above for the gas-phase reactions (20 ppm CO of car exhaust diluted with outdoor air and a chamber mean residence time of 30 min, the chamber achieved a relatively stable SOA mass concentration of approximately $40 \mu\text{g m}^{-3}$ after 5–6 h of irradiation time. Figure 4 shows the average SOA mass concentration and its variability (standard error) from 5 experiments conducted under the same experimental conditions.

In a related set of experiments, the CO introduced into the chamber was adjusted to be approximately 10 ppm, while the mean residence time in the chamber was maintained at 30 min. With CO concentration reduced to one half as much, the SOA yield was on average $10 \mu\text{g m}^{-3}$ lower than the SOA formed at 20 ppm CO, reaching only $30.2 \pm 6.1 \mu\text{g m}^{-3}$. We observed that a decrease in the amount of CO resulted in a decrease in the amount of SOA formed in the chamber. This may be due to the corresponding decreased amount of VOCs concentrations in the chamber. In such case, this is confirmation of our assumption (made above) that CO serves as a surrogate for VOCs.

Residence/irradiation time effect

Figure 5 shows the effect of residence/irradiation time on the evolution of the secondary particle size distribution. After a steady-state CO concentration of 20 ppm was reached, the

chamber was capped to simulate a static condition and the lamps were turned on. The SMPS was used to sample every hour at 0.3 L min^{-1} . In the absence of seed aerosol, the initial burst in the first hour with particles forming in the ultrafine region around 30 nm is mainly due to nucleation (Cocker et al., 2001b).

The evolution of the particle count size distribution indicates that there was a slow coagulation process, as well as particle growth due to condensation/partitioning of freshly formed oxidized (semivolatile) organics onto surfaces, during the course of 0–7 h of elapsed residence/ irradiation time.

During the same static chamber experiment, we also examined the effect of residence/ irradiation time on secondary aerosol mass formation. Figure 6 shows that the highest SOA mass yield occurs approximately 2 h after irradiation. As suggested by Figure 5, the dominant SOA particle size formation mechanisms in the laboratory chamber were most likely nucleation and subsequent slow coagulation and condensation. These results indicate that a longer residence/irradiation time (longer than one hour) might be needed to achieve total mass concentrations that would be adequate for toxicological testing.

VOCs consumption

The fractions of selected gasoline-associated VOCs that reacted in the chamber with the lamps on ranged from 3.8 to 19.9% (see Table 1). It has been shown that a given aromatic compound may have higher reactivity than some other aromatics, but lower SOA-forming potential. For example, Carter (1994) has shown that benzene has the lowest relative reactivity in the adjusted NO_x scales (3.8% reacted in our chamber), while *m*-xylene has the highest (almost 20% reacted in our chamber). Although our results show that more of the *m*-xylene than toluene reacted in the chamber, Odum et al. (1997b) have shown that toluene results in higher SOA yields than *m*-xylene. The chamber was operated in a dynamic mode with a short mean residence time. Because fresh VOCs were being added constantly and the rate of VOCs reactions was lower than the rate of VOCs replenishment, the concentrations downstream would be relatively high.

EC/OC formation

Results from the EC/OC analysis are presented in Table 2. Four OC fractions at temperature ramping between $\sim 25^\circ\text{C}$ and 550°C are reported. The average differences in total OC concentrations between downstream and upstream concentrations for all three sets of experiments clearly indicate the there is SOA formation in the chamber during irradiation of vehicular primary gasphase precursors. Shorter mean residence time (30 min) in the chamber results in higher particle mass formation. The substantially greater amounts downstream of the chamber of OC2 and OC3 fractions, for temperatures between 120°C and 4500°C , show that the secondary aerosol has significantly more very low-volatility organic species than the primary aerosol. This material generally has higher molecular weight and is more polar than the higher volatility species that are released at lower temperatures, consistent with the expected properties of SOA compounds.

Seed aerosol effect

To test for the effect of seed aerosol surface on the formation of SOA, 12 experiments were conducted using HGS as the seed aerosol and another 12 experiments were conducted using MSHA. For this purpose, the experiments were conducted by varying the seed aerosol concentration between low and high in combination with variation in the mean residence time in the chamber and in the CO concentration from the diluted car exhaust. The primary particle mass concentration emitted by the car was negligible.

In the seed aerosol experiments (see Table 3), following stabilization of the CO in the chamber (ranged between 2.0 ppm and 26.4 ppm), addition of the seed aerosol was started. When a steady-state baseline seed aerosol mass concentration was reached (ranged between $42.4 \mu\text{g m}^{-3}$ and $804.1 \mu\text{g m}^{-3}$), the lamps were turned on to initiate the photochemical reactions. After a 180-min irradiation with the lamps on, the SOA formed in the chamber was measured (ranged between $21.5 \mu\text{g m}^{-3}$ and $437.8 \mu\text{g m}^{-3}$). The mean residence time in the chamber was set at either 50 or 100 min.

The relationship between the steady-state SOA yield concentration (C_S) formed in our chamber with the lamps on and the varying parameters in our tests was examined. We developed an empirical equation by linear regression (SAS Institute Inc., Cary, NC) that shows a logarithmic relationship between SOA and (1) the seed aerosol mass concentration, (2) the CO concentration (surrogate for VOCs concentration), with an $R^2 = 0.84$. The type of seed aerosol (hollow glass spheres or MSHA) was not significant when included in the model. It should be noted that both types of seed aerosol used are inert aerosols. A reactive seed aerosol might behave differently. In this work, the SOA yield formed was only dependent on the amount of seed aerosol used. The empirical model is shown in Equation (9):

$$C_{\text{SOA}} = \exp(3.47 + 3.05 \cdot 10^{-3} \cdot C_{\text{seed}} + 2.86 \cdot 10^{-2} \cdot C_{\text{CO}}) \quad (8)$$

where C_{SOA} : mass concentration ($\mu\text{g m}^{-3}$); C_{seed} : seed aerosol mass concentration ($\mu\text{g m}^{-3}$); C_{CO} : carbon monoxide concentration (ppm).

Seed aerosol addition had a significant effect on the SOA yield formed. As shown earlier, at an average of 10 ppm of CO in the chamber, the experiments without seed aerosol yielded an average $30 \mu\text{g m}^{-3}$ of SOA formed, while the seed aerosol experiments with the same CO concentration yielded approximately an average of $70 \mu\text{g m}^{-3}$. The same effect was observed at a higher concentration of approximately 20 ppm of CO. At that concentration, the experiments without seed aerosol yielded an average of $40 \mu\text{g m}^{-3}$ of SOA formed, while the seed aerosol experiments yielded an average of $105 \mu\text{g m}^{-3}$ of SOA formed. This was as expected. In the experiments with no seed aerosol, the primary mechanisms for particle formation are nucleation and coagulation of the ultrafine particles (Cocker et al., 2001a), consistent with the evolution of the particle size distribution with increasing residence/irradiation time shown in Figure 5. The seed particle surface area competes with the chamber walls for vehicular gases to condense on particles or become lost on the walls, respectively. The higher the seed particle concentration, the greater the surface area and consequently the higher the gas molecules concentration will condense on the particles. The mean residence time did not seem to play an important role in the formation of SOA for the experiments with either type of seed aerosol. Having the seed aerosol provide a surface for condensation of gas-phase species minimizes the roles of nucleation and coagulation effects that make the mean residence time an important parameter in the chamber tests described above with the car exhaust only and without seed aerosol.

***In vivo* chemiluminescence**

Exposure doses for these toxicological studies were $\text{MSHA} = 363.0 \pm 66.0 \mu\text{g m}^{-3}$ and $\text{MSHA} + \text{SOA} = 211.5 \pm 95.3 \mu\text{g m}^{-3}$. *In vivo* chemiluminescence was assessed at the surface of the heart and lung. No differences were observed between filtered air controls and either primary or secondary particle exposures for *in vivo* chemiluminescence of the heart (data not shown). However, *in vivo* chemiluminescence of the lung showed clear differences between exposures. There was no significant difference between filtered air controls and exposures with lamps off in the MSHA scenario confirming the lack of toxicity with MSHA aerosols. With lamps on and with the formation of secondary particles on the MSHA

particles, a significant increase in lung chemiluminescence versus filtered air controls was observed as well as between scenarios as shown in Figure 7.

Conclusions

The laboratory chamber tests investigated the photochemical reactivity of car exhaust from a single vehicle, diluted with ambient air. Once the UV lamps were turned on, photochemical reactions were initiated, without the addition of any accelerant, resulting in a rapid NO depletion, NO₂ formation, and O₃ accumulation. We determined the conditions needed to produce an adequate amount of SOA mass for use with an in-laboratory animal toxicological study (complete manuscript in preparation), and in this report we show a significant response to SOA in the lungs of normal rats at a concentration less than that of the MSHA without formation of SOA. A stable SOA concentration of approximately 40 µg m⁻³ at a chamber mean residence time of 30 min was achieved. This relatively short mean residence time provided adequate chamber flow output for both particle characterization and animal exposures. The chamber was operated as a continuous flow reactor for toxicological tests with animal exposures. The information gathered from this laboratory evaluation was used to inform the design and development of a significantly larger reaction chamber that would generate SOA mass from urban highway tunnel fleet emissions in a real field setting. The field project has been completed and the manuscript is in preparation.

Acknowledgments

This publication was made possible by USEPA grants R-832416 and RD 83479801. Its contents are solely the responsibility of the grantee and do not necessarily represent the official views of the USEPA. Further, USEPA does not endorse the purchase of any commercial products or services mentioned in the publication. This work was also supported by the Harvard NIEHS Center for Environmental Health (grant P30ES000002). We thank Dr. Stephen Rudnick for reading the manuscript and providing helpful suggestions. We also thank Dr. Choong-Min Kang and Samuel Pueringer for the analytical support. Technical assistance was provided by John Tosti, Vivian Hatakeyama, Brenno Gomes, and Yasser Calil.

References

- Carter WPL. Development of ozone reactivity scales for volatile organic compounds. *J Air Waste Manage Assoc.* 1994; 44:881–899.
- Carter WPL, Luo D, Malkina IL, Pierce JA. Environmental chamber studies of atmospheric reactivities of volatile organic compounds. Effects of varying chamber and light source. 1995 Final Report.
- Chow JC, Watson JG, Pritchett LC, Pierson WR, Frazier CA, Purcell RG. The DRI thermal/optical reflectance carbon analysis system: description, evaluation and applications in U.S. air quality studies. *Atmos Environ.* 1993; 27A:1185–1201.
- Cocker DR III, Mader BT, Kalberer M, Flagan RC, Seinfeld JC. The effect of water on gas-particle partitioning of secondary organic aerosol, II *m*-Xylene and 1,3,5-trimethylbenzene photooxidation systems. *Atmos Environ.* 2001a; 35:6073–6085.
- Cocker DR 3rd, Flagan RC, Seinfeld JH. State-of-the-art chamber facility for studying atmospheric aerosol chemistry. *Environ Sci Technol.* 2001b; 35:2594–2601. [PubMed: 11432570]
- Crump JG, Seinfeld JH. Turbulent deposition and gravitational sedimentation of an aerosol in a vessel of arbitrary shape. *J Aerosol Sci.* 1981; 12:405–415.
- Dockery DW, Pope CA 3rd. Acute respiratory effects of particulate air pollution. *Annu Rev Public Health.* 1994; 15:107–132. [PubMed: 8054077]
- Dockery DW, Pope CA 3rd, Xu X, Spengler JD, Ware JH, Fay ME, Ferris BG Jr. Speizer FE. An association between air pollution and mortality in six U.S. cities. *N Engl J Med.* 1993; 329:1753–1759. [PubMed: 8179653]

- Feilberg A, Nielsen T, Binderup ML, Skov H, Poulsen MWB. Observations of the effect of atmospheric processes on the genotoxic potency of airborne particulate matter. *Atmos Environ*. 2002; 36:4617–4625.
- Finlayson-Pitts, BJ.; Pitts, JN. *Atmospheric Chemistry*. New York: John Wiley & Sons; 1986.
- Fraser MP, Cass GR, Simoneit BRT. Gas-phase and particlephase organic compounds emitted from motor vehicle traffic in a Los Angeles roadway tunnel. *Environ Sci Technol*. 1998; 32:2051–2060.
- Godleski, JJ.; Diaz, EA.; Lemos, M.; Long, M.; Ruiz, P.; Gupta, T.; Kang, CM.; Coull, B. Toxicological Evaluation of Realistic Emission Source Aerosols (TERESA)-power plant studies: assessment of cellular responses. *Inhal Toxicol* in press; 2011.
- Godleski, JJ.; Koutrakis, P.; Kang, CM.; Diaz, EA.; Rohr, AC. Toxicological Evaluation of Realistic Emission Source Aerosols (TERESA): Introduction and overview. *Inhal Toxicol* in press; 2011.
- Gurgueira SA, Lawrence J, Coull B, Murthy GG, González-Flecha B. Rapid increases in the steady-state concentration of reactive oxygen species in the lungs and heart after particulate air pollution inhalation. *Environ Health Perspect*. 2002; 110:749–755. [PubMed: 12153754]
- Izumi K, Fukuyama T. Photochemical aerosol formation from aromatic-hydrocarbons in the presence of NO_x. *Atmos Environ*. 1990; 24:1433–1441.
- Kang, CM.; Gupta, T.; Ruiz, PA.; Wolfson, JM.; Ferguson, ST.; Lawrence, JE.; Rohr, AC.; Godleski, J.; Koutrakis, P. Aged particles derived from emissions of coal-fired power plants: the TERESA field results. *Inhal Toxicol* in press; 2011.
- Kirchstetter TW, Singer BC, Harley RA, Kendall GR, Chan W. Impact of oxygenated gasoline use on California light duty vehicle emissions. *Environ Sci Technol*. 1996; 30:661–670.
- Kleindienst TE, Conner TS, McIver CD, Edney EO. Determination of secondary organic aerosol products from the photooxidation of toluene and their implications in ambient PM_{2.5}. *J Atmos Chem*. 2004; 47:79–100.
- Kleindienst TE, Smith DF, Li W, Edney EO, Driscoll DJ, Speer RE, Weathers WS. Secondary organic aerosol formation from the oxidation of aromatic hydrocarbons in the presence of dry submicron ammonium sulfate. *Atmos Environ*. 1999; 33:3669–3681.
- Laden F, Neas LM, Dockery DW, Schwartz J. Association of fine particulate matter from different sources with daily mortality in six U.S. cities. *Environ Health Perspect*. 2000; 108:941–947. [PubMed: 11049813]
- Lim HJ, Turpin BJ. Origins of primary and secondary organic aerosol in Atlanta: results of time-resolved measurements during the Atlanta Supersite Experiment. *Environ Sci Technol*. 2002; 36:4489–4496. [PubMed: 12433156]
- McDonald JD, Harrod KS, Seagrave J, Seilkop SK, Mauderly JL. Effects of low sulfur fuel and a catalyzed particle trap on the composition and toxicity of diesel emissions. *Environ Health Perspect*. 2004; 112:1307–1312. [PubMed: 15345344]
- Ng NL, Kroll JH, Keywood MD, Bahreini R, Varutbangkul V, Flagan RC, Seinfeld JH, Lee A, Goldstein AH. Contribution of first-versus second-generation products to secondary organic aerosols formed in the oxidation of biogenic hydrocarbons. *Environ Sci Technol*. 2006; 40:2283–2297. [PubMed: 16646465]
- Nikolaou K, Masplet P, Mouvier G. Sources and chemical reactivity of polynuclear aromatic hydrocarbons in the atmosphere? A critical review. *Sci Total Environ*. 1984; 32:103–132.
- Odum JR, Jungkamp TP, Griffin RJ, Flagan RC, Seinfeld JH. The atmospheric aerosol-forming potential of whole gasoline vapor. *Science*. 1997; 276:96–99. [PubMed: 9082994]
- Odum JR, Jungkamp TPW, Griffin RJ, Forstner HJL, Flagan RC, Seinfeld JH. Aromatics, reformulated gasoline, and atmospheric organic aerosol formation. *Environ Sci Technol*. 1997b; 31:1890–1897.
- Peters A, von Klot S, Heier M, Trentinaglia I, Hörmann A, Wichmann HE, Löwel H. Exposure to traffic and the onset of myocardial infarction. *N Engl J Med*. 2004; 351:1721–1730. Cooperative Health Research in the Region of Augsburg Study Group. [PubMed: 15496621]
- Pierce JR, Engelhart GJ, Hidebrandt L, Weitkamp EA, Pathak RK, Donahue NM, Robinson AL, Adams PJ, Pandis SN. Constraining particle evolution from wall losses, coagulation and condensation-evaporation in smog chamber experiments: optimal estimation based on size distribution measurements. *Aerosol Sci Technol*. 2008; 42:1001–1015.

- Pierson WR, Gertler AW, Robinson NF, Sagebiel JC, Zelinska B, Bishop GA, Stedman DH, Zweidinger RB, Ray WR. Real-world automotive emissions—summary of studies in the Fort McHenry and Tuscarora mountain tunnels. *Atmos Environ*. 1996; 30:2233–2256.
- Pope CA 3rd, Burnett RT, Tun MJ, Calle EE, Krewski D, Ito K, Thurston GD. Lung cancer, cardiopulmonary mortality, and long-term exposure to fine particulate air pollution. *JAMA*. 2002; 287:1132–1141. [PubMed: 11879110]
- Rogak SN, Pott U, Dann T, Wang D. Gaseous emissions from vehicles in a traffic tunnel in Vancouver, British Columbia. *J Air Waste Manag Assoc*. 1998; 48:604–615. [PubMed: 9706040]
- Ruiz PA, Gupta T, Kang CM, Lawrence JE, Ferguson ST, Wolfson JM, Rohr AC, Koutrakis P. Development of an exposure system for the toxicological evaluation of particles derived from coal-fired power plants. *Inhal Toxicol*. 2007; 19:607–619. [PubMed: 17510834]
- Ruiz PA, Lawrence JE, Ferguson ST, Wolfson JM, Koutrakis P. A counter-current parallel-plate membrane denuder for the non-specific removal of trace gases. *Environ Sci Technol*. 2006; 40:5058–5063. [PubMed: 16955907]
- Ruiz PA, Lawrence JE, Wolfson JM, Ferguson ST, Gupta T, Kang CM, Koutrakis P. Development and evaluation of a photochemical chamber to examine the toxicity of coal-fired power plant emissions. *Inhal Toxicol*. 2007; 19:597–606. [PubMed: 17510833]
- Sander SP, Friedl RR, Golden DM, Kurylo MJ, Huie RE, Orkin VL, Moortgat GK, Ravishankara AR, Kolb CE, Molina MJ, Finlayson-Pitts BJ. Chemical kinetics and photochemical data for use in atmospheric studies. Evaluation no. 14, Jet Propulsion Laboratory publication. 2003:02–25.
- Savage ST, Lawrence J, Katz T, Stearns RC, Coull BA, Godleski JJ. Does the Harvard/U.S. Environmental Protection Agency Ambient Particle Concentrator change the toxic potential of particles? *J Air Waste Manag Assoc*. 2003; 53:1088–1097.
- Schwartz J. Air pollution and children's health. *Pediatrics*. 2004; 113:1037–1043. [PubMed: 15060197]
- Seagrave J, Mauderly JL, Seilkop SK. *In vitro* relative toxicity screening of combined particulate and semivolatile organic fractions of gasoline and diesel engine emissions. *J Toxicol Environ Health Part A*. 2003; 66:1113–1132. [PubMed: 12854533]
- Seinfeld, JH.; Pandis, SN. From air pollution to climate change. New York: John Wiley & Sons; 2006. Atmospheric chemistry and physics.
- Zafonte L, Rieer PL, Holmes. Nitrogen-dioxide photolysis in Los Angeles atmosphere. *Environ Sci Technol*. 1977; 11:483–487.
- Zielinska B, Samy S, McDonald JD, Seagrave J. Atmospheric transformation of diesel emissions. *Res Rep Health Eff Inst*. 2010:5–60. HEI Health Review Committee. [PubMed: 20572366]

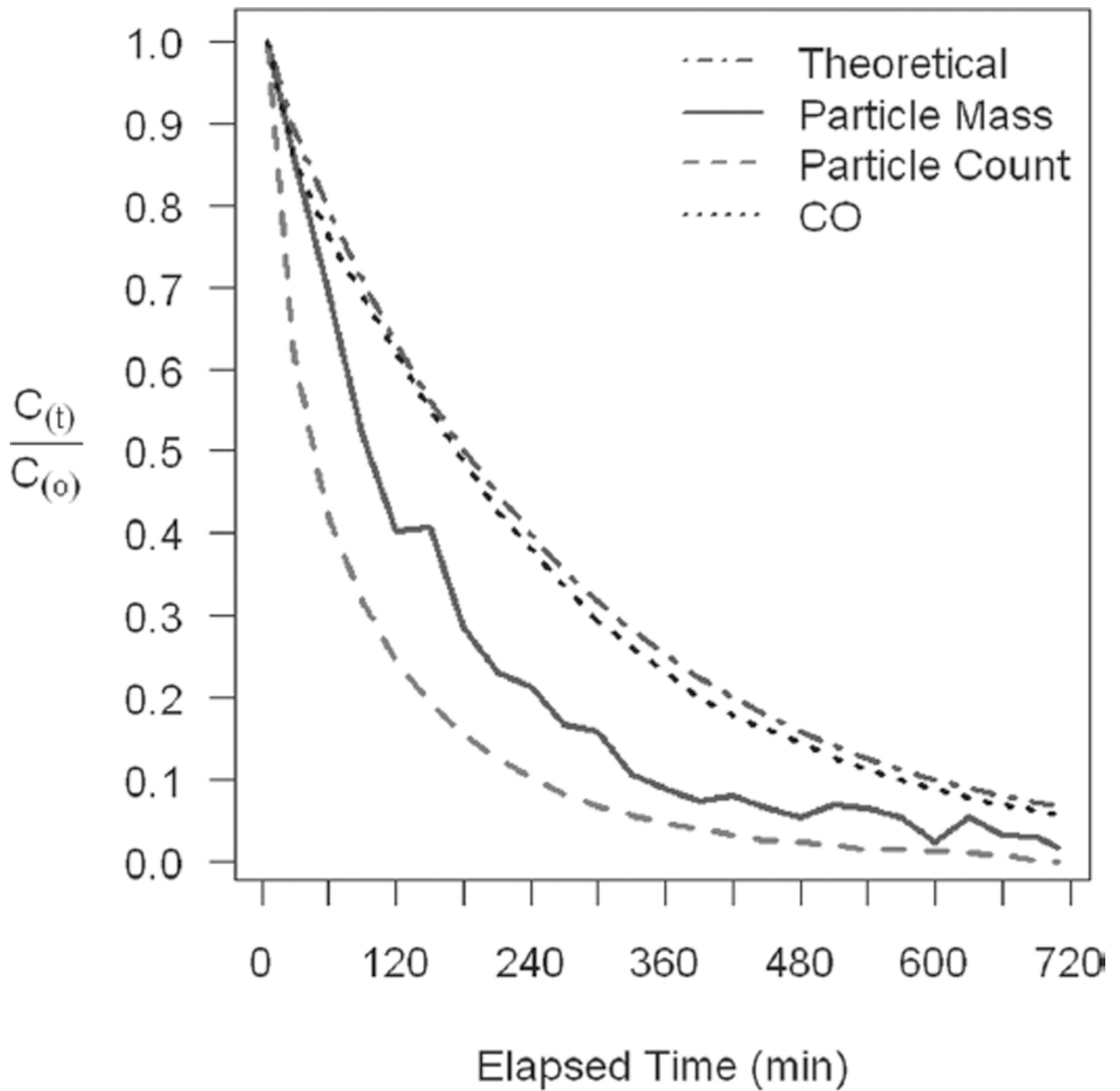


Figure 2. Particle and CO decay curves in the chamber. (See colour version of this figure online at www.informahealthcare.com/iht)

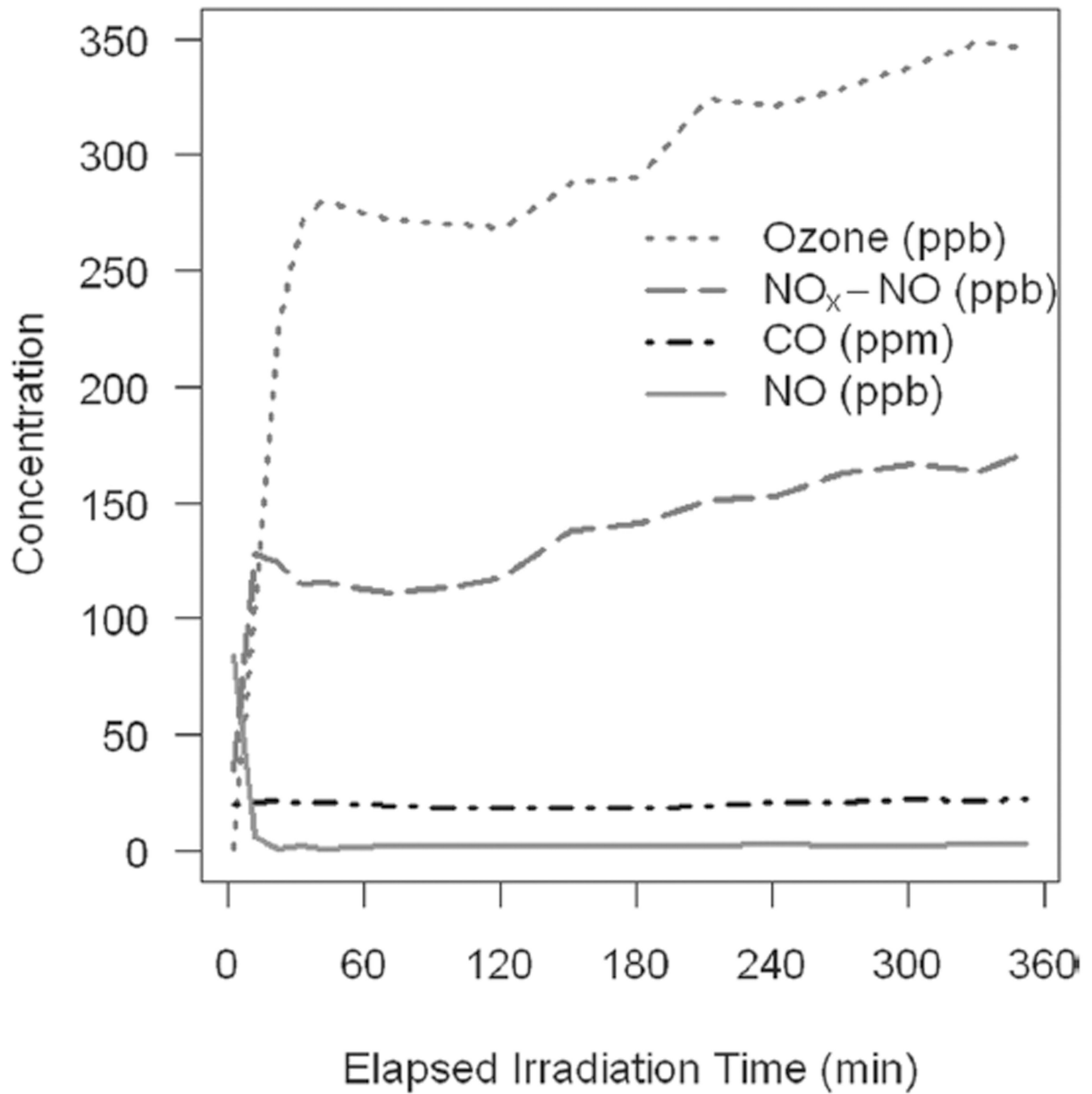


Figure 3. Gas-phase reactions in the well-mixed flow reactor. (See colour version of this figure online at www.informahealthcare.com/ihl)

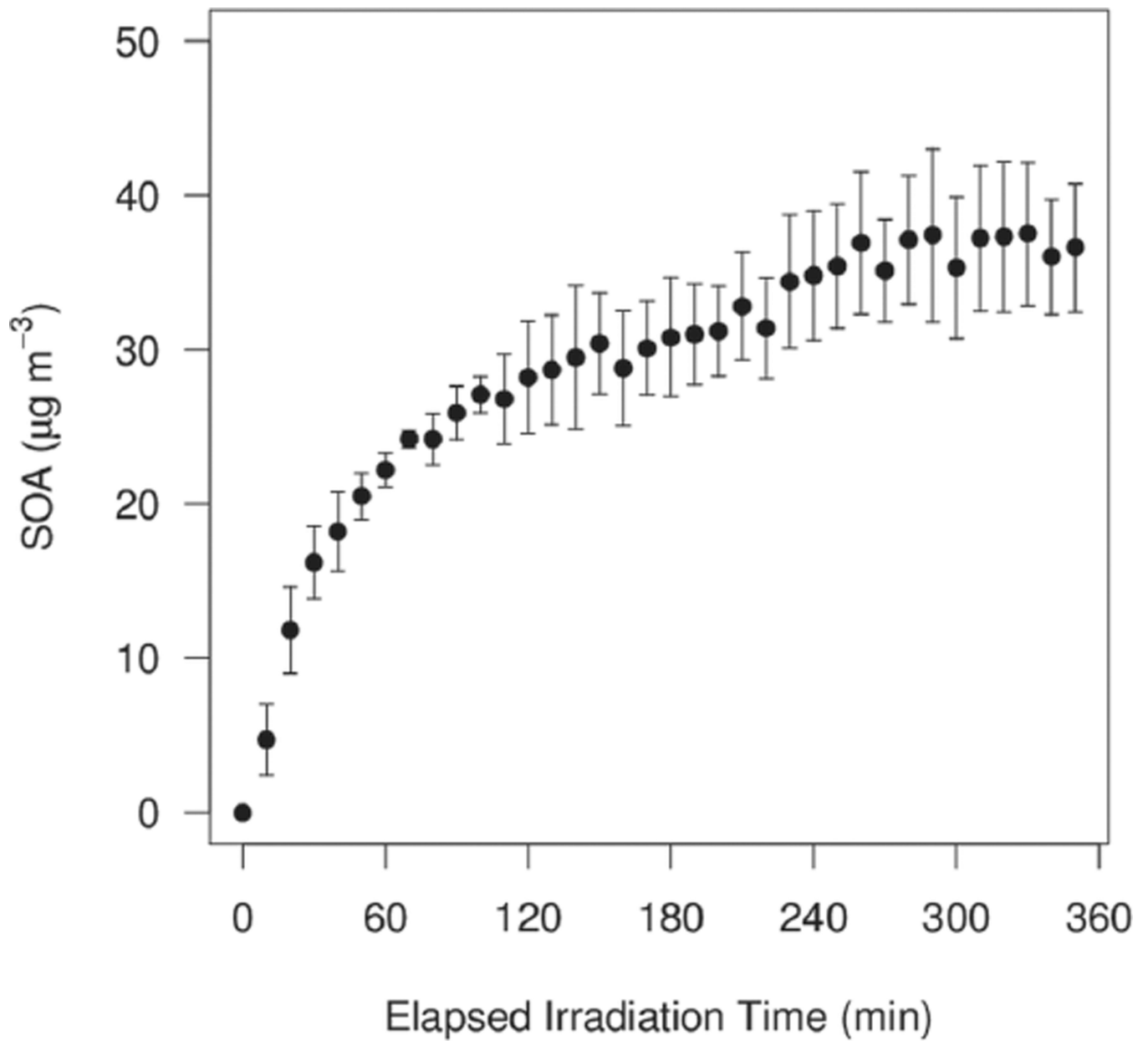


Figure 4. Secondary organic aerosol formation at 20 ppm of CO and a mean residence time of 30 min. SOA, secondary organic aerosol.

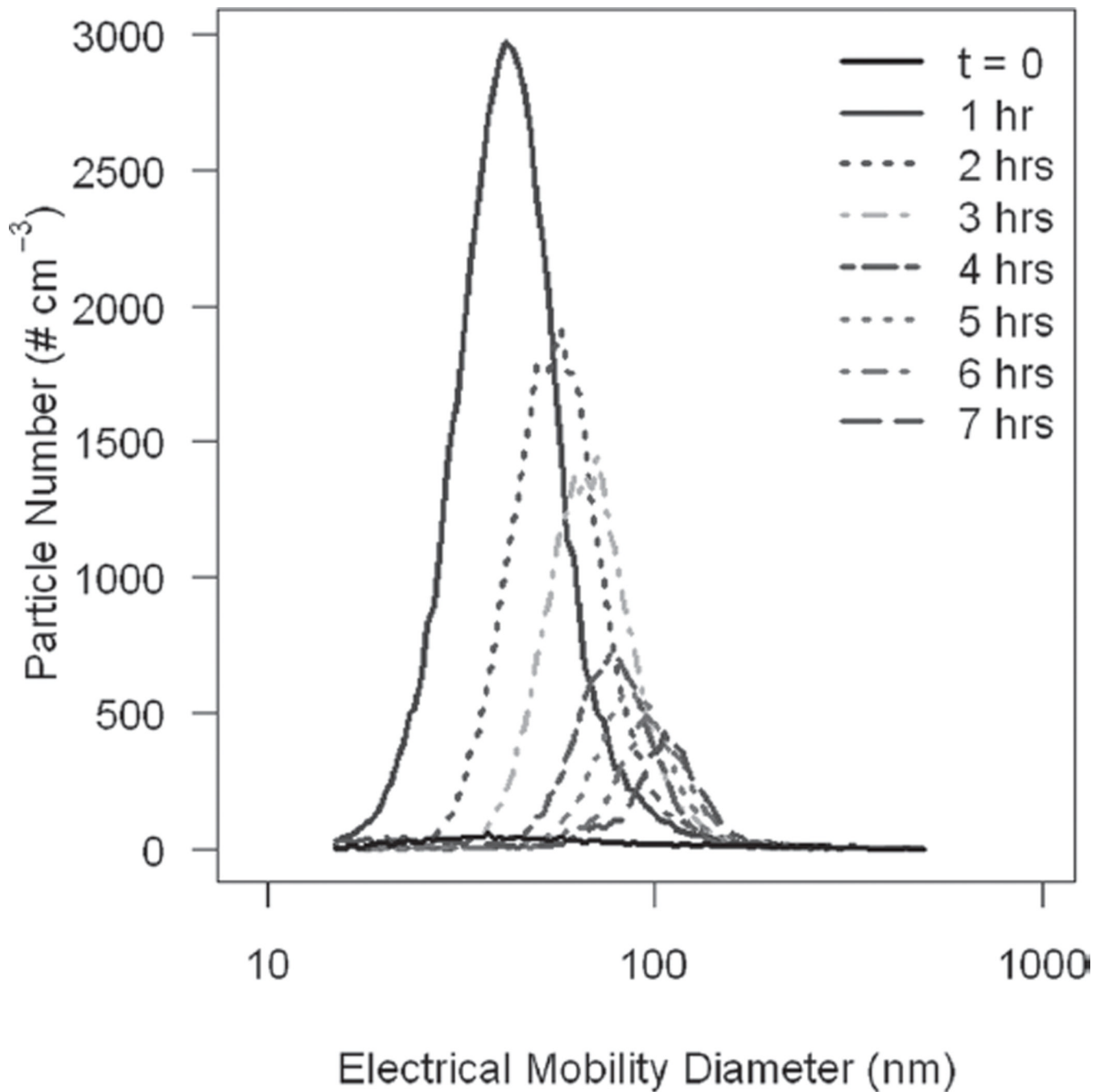


Figure 5. The effect of residence/irradiation time on particle size. (See colour version of this figure online at www.informahealthcare.com/ihf)

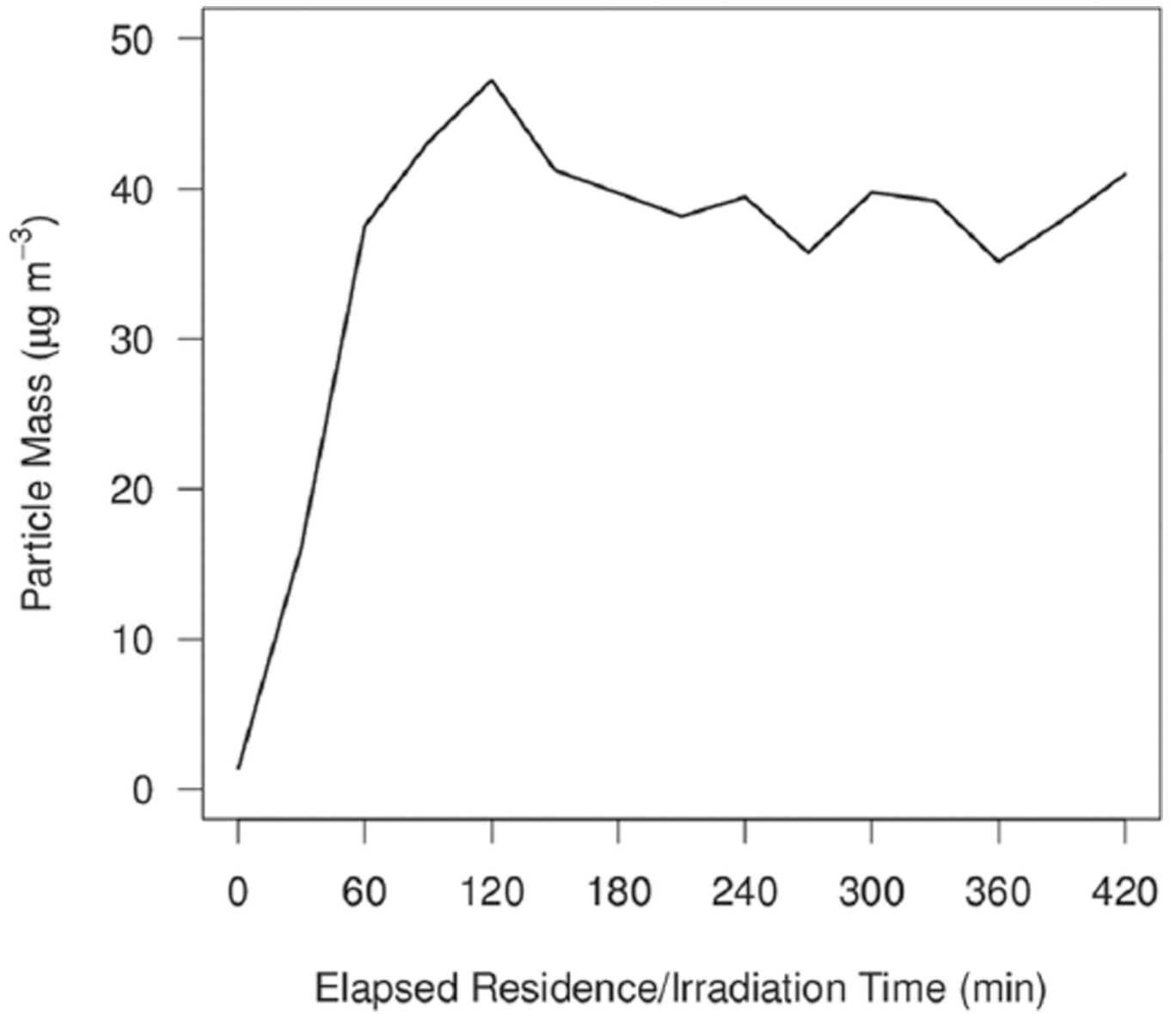


Figure 6.
The effect of residence/irradiation time on particle mass.

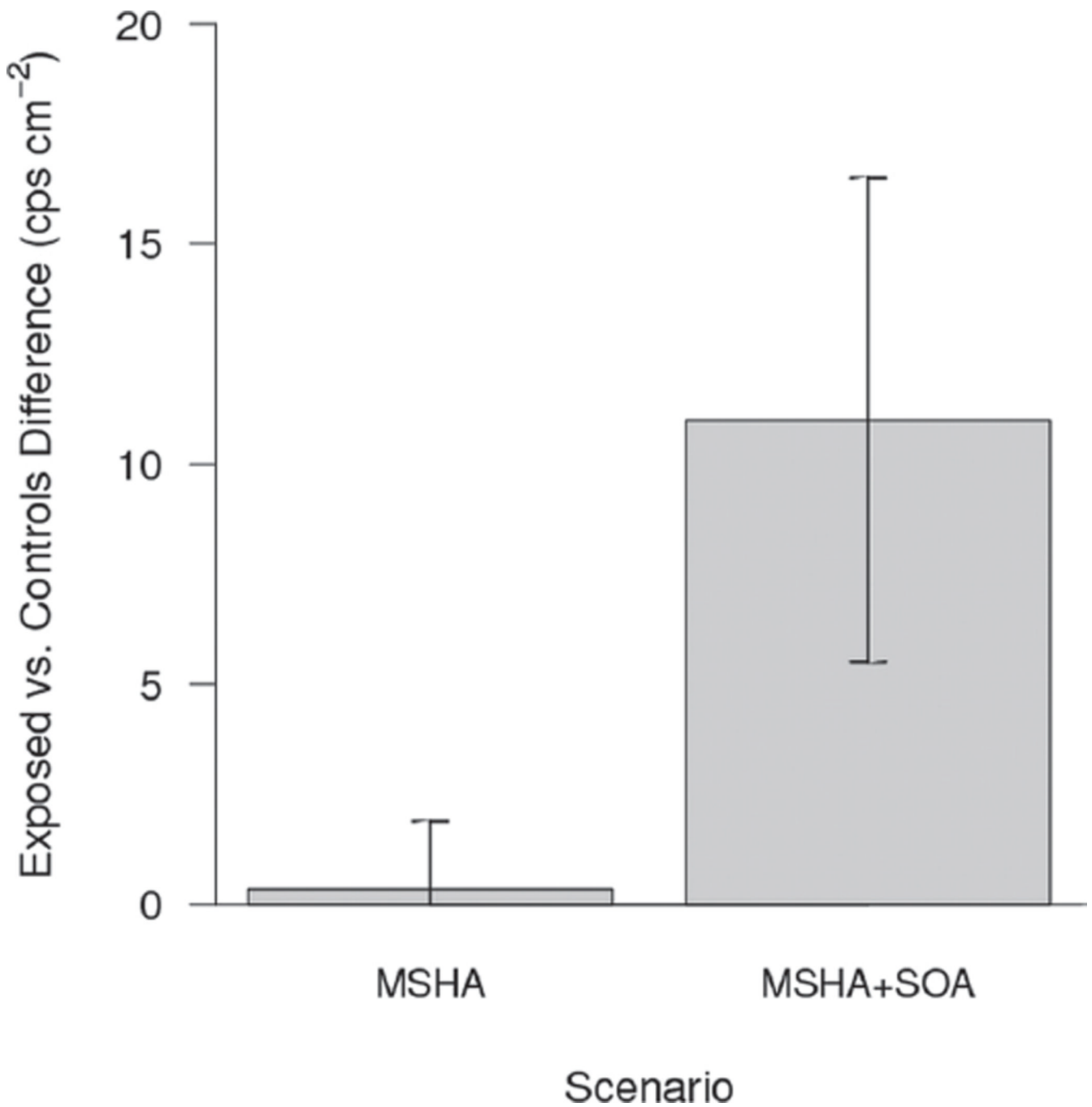


Figure 7. The difference between MSHA+SOA and filtered air controls and the differences between scenarios are both $p < 0.05$. MSHA, Mt Saint Helens Ash; SOA, secondary organic aerosol. (See colour version of this figure online at www.informahealthcare.com/ihf)

Table 1

Amounts of reacted VOCs.

	Upstream of chamber, mean (±SD) (ppb)	Downstream of chamber, mean (±SD) (ppb)	Reacted (%)
Benzene	60.7 ± 2.9	58.4 ± 2.0	3.8
Ethylbenzene	10.3 ± 1.1	9.7 ± 1.0	5.4
Toluene	49.8 ± 8.8	44.6 ± 5.0	10.3
<i>o</i> -Xylene	12.4 ± 1.4	10.9 ± 0.9	11.8
<i>m/p</i> -Xylene	32.1 ± 3.1	27.8 ± 2.9	13.4

During this experiment: CO: 20.6 ± 0.6 ppm, NO_x-NO: 148.3 ± 12.9 ppb, O₃: 325.5 ± 14.0 ppb, SMPS: 30.6 ± 2.1 μg m⁻³, CPC 55,000 ± 6,000 # cm⁻³ $T_{\text{res}} = 30$ min.

CO, carbon monoxide; CPC, Condensation Particle Counter; SMPS, Scanning Mobility Particle Sizer; T_{res} , residence time; VOC, volatile organic compound.

Table 2

Organic carbon analysis.

	10 ppm CO and 30 min residence time, mean (\pm SD) ($\mu\text{g m}^{-3}$)		10 ppm CO and 60 min residence time, mean (\pm SD) ($\mu\text{g m}^{-3}$)		20 ppm CO and 30 min residence time, mean (\pm SD) ($\mu\text{g m}^{-3}$)	
	Upstream	Downstream	Upstream	Downstream	Upstream	Downstream
Total OC	24.2 \pm 7.0	77.7 \pm 7.6	16.9 \pm 3.9	539 \pm 10.2	20.4 \pm 4.7	50.6 \pm 15.2
OC1	0.7 \pm 0.3	2.4 \pm 0.5	0.5 \pm 0.1	2.5 \pm 0.3	1.0 \pm 0.4	2.0 \pm 0.1
OC2	15.6 \pm 5.9	37.5 \pm 6.1	10.2 \pm 3.4	22.3 \pm 4.3	7.3 \pm 0.6	21.8 \pm 5.0
OC3	5.8 \pm 0.6	25.6 \pm 2.1	4.6 \pm 0.6	20.3 \pm 3.5	10.1 \pm 2.9	18.1 \pm 7.0
OC4	1.3 \pm 0.1	7.4 \pm 0.6	0.9 \pm 0.1	5.7 \pm 1.4	1.5 \pm 0.5	5.0 \pm 1.8

Temperature range for each OC fraction: ~25–120°C (OC1); 120–250°C (OC2); 250–450°C (OC3); and 450–550°C (OC4).

Table 3

Seed aerosol experimental data.

CO ppm	Seed aerosol		SOA	Residence time
	type	$\mu\text{g m}^{-3}$	$\mu\text{g m}^{-3}$	min
2.0	HGS	294.8	48.9	100
3.0	MSHA	603.0	222.7	50
3.1	MSHA	60.2	21.5	50
4.3	HGS	42.4	35.0	100
4.6	HGS	341.0	72.7	50
5.2	MSHA	129.0	70.7	50
5.5	MSHA	128.3	77.6	50
5.9	MSHA	636.0	378.3	50
6.2	HGS	62.0	46.8	50
6.9	MSHA	804.1	437.8	50
6.9	MSHA	119.9	67.9	50
7.3	MSHA	140.9	69.0	50
7.4	MSHA	132.2	77.2	50
9.0	MSHA	218.6	87.9	50
9.0	MSHA	156.0	92.2	50
9.3	MSHA	626.6	329.2	50
9.5	HGS	104.8	89.2	50
11.3	HGS	154.5	71.7	50
11.8	HGS	170.5	64.0	100
13.7	HGS	174.2	71.7	100
20.7	HGS	228.5	103.0	50
20.9	HGS	62.3	73.5	100
26.0	HGS	370.0	143.7	100
26.4	HGS	83.7	101.5	50

HGS, hollow glass sphere; MSHA, Mt Saint Helens Ash; SOA, secondary organic aerosol.